Available online at www.sciencedirect.com
ScienceDirect
Vacuum 80 (2006) 1126–1131
VACUUM
SURFACE ENGINEERING, SURFACE INSTRUMENTATION & VACUUM TECHNOLOGY
www.elsevier.com/locate/vacuum

Synthesis of functional nanoassemblies in reactive plasmas

K. Ostrikov[a,b,*], J.D. Long[b], P.P. Rutkevych[b], S. Xu[b]

[a]School of Physics, The University of Sydney, Sydney NSW 2006, Australia
[b]Plasma Sources and Applications Center, NIE, NTU, 1 Nanyang Walk, 637616 Singapore, Singapore

Abstract

Synthesis of various functional nanoassemblies, by using a combination of low-pressure reactive plasma-enhanced chemical deposition and plasma-assisted rf magnetron sputtering deposition is reported. This paper details how selective generation and manipulation of the required building blocks and management of unwanted nanoparticle contaminants, can be used for plasma-aided nanofabrication of carbon nanotip microemitter structures, ultra-high aspect ratio semiconductor nanowires, ordered quantum dot arrays, and microporous hydroxyapatite bioceramics. Emerging challenges of the plasma-aided synthesis of functional nanofilms and nanoassemblies are also discussed.

Keywords: Nanoassembly; Deterministic nanofabrication; PECVD; Reactive plasma; Nano- and biomaterials

1. Introduction

Various plasma-based processes and processing tools currently find numerous applications for nanofabrication of numerous functional nanoassemblies, nanopatterns and nanostructured materials owing to the unique ability of the plasma environment to dissociate and change energetic states of essentially neutral gas feedstock [1–5]. The ability to manipulate the number densities, energies, and fluxes of the entire range of the plasma species becomes a critical issue of the plasma processing [4,5]. The above plasma species can vary in size from atoms and simple ions (in the subnanometer size range) to macromolecules and fine crystallites, the latter usually exceeding 1 nm in size. Generation and manipulation of a wide range of reactive species becomes indispensable for a number of emerging plasma applications in nanoscience and nanotechnology [5,6]. Indeed, a proper choice of the process parameters is crucial to meeting the expected industrial standards, for example, in microelectronics and optoelectronics that heavily rely on nanotech solutions. This is particularly critical for the plasma-aided fabrication of nanofilms and nanoassemblies (NAs), which at present merely relies on inefficient and expensive "trial and error" practices.

The key to solve this problem is to tailor the elementary gas-phase and surface kinetics and chemistry that control generation and dynamics of the working reactive species in the plasma. This can eventually result in the achievement of greater control and predictability of various plasma-assisted industrial processes. The examples of the above processes include but are not limited to deep-micron etching, deposition of barrier and stripping of photoresistant layers in microelectronic technologies; plasma-assisted synthesis of functional (from protective wear-resistant metal coatings to biodegradable polymeric films) coatings; environmental remediation and cleaning of fouled surfaces; radio-communications; inactivation of airborne bacteria; plasma welding/cutting, and several others. To this end, it is very important to develop most efficient approaches, as well as suitable plasma facilities and process specifications. Here, we introduce the "cause and effect" approach based on selective generation and manipulation of building units (BUs) of the targeted nanofilms and nanostructures. We also describe the integrated plasma-aided nanofabrication facility (IPANF) and discuss specific examples of synthesis of functional nanoassemblies in reactive plasmas.

*Corresponding author. School of Physics, The University of Sydney, Sydney NSW 2006, Australia. Tel.: +61 293 516 081; fax: +61 2 9351 7726.
E-mail address: K.Ostrikov@physics.usyd.edu.au (K. Ostrikov).

0042-207X/$ - see front matter © 2006 Elsevier Ltd. All rights reserved.
doi:10.1016/j.vacuum.2006.01.025

2. "Cause and effect" approach

Our approach for the assembly of various nanostructured films and nanoassemblies capitalizes on the choice, generation, and manipulation of the required building units in the ionized gas phase. The four main milestones, incorporated in the logic flow chart (Fig. 1(a)) of the advocated "cause and effect" approach are: (i) generation of the required BUs in the ionized gas phase; (ii) surface preparation for deposition and incorporation of the BUs; (iii) transport of the BUs through the plasma sheath to the deposition surface; and (iv) stacking of BUs into the required nanoassembly or film being grown. To this end, it is important to emphasize that chemically active plasma environments can generate the entire range of BUs ranging from atoms, ions, molecules and radicals through to nanoclusters, fine nucleates, nanoparticles, and nanoparticle agglomerates. Depending on the requirements for the nanofilm of nanostructure, specific BUs are chosen in each particular process. In the nanofabrication of single crystalline carbon nanotip (CNT) structures, radical CH_3 and cation CH_3^+ are the BUs, whereas SiC quantum dot (QD) structures require Si and C atoms and ions as BUs. While the BUs are transported to the surface from the plasma bulk through the plasma sheath, the deposition surface is suitably prepared for landing and stacking of the BUs. Another possibility is that the BUs are delivered to the substrate and then migrate to the growth site, where they insert into the nanoassemblies being grown. Finally, appropriate control of the fluxes and energy of the BUs, and surface temperature enables one to appropriately stack the BUs into the nanopattern or the nanofilm being grown. More details of the use of reactive plasmas in nanofabrication can be found elsewhere [6]. Below, by using the plasma diagnostic, nanofilm characterization, and numerical simulation, we show the possibility to achieve the desired structural and other parameters of the targeted NAs.

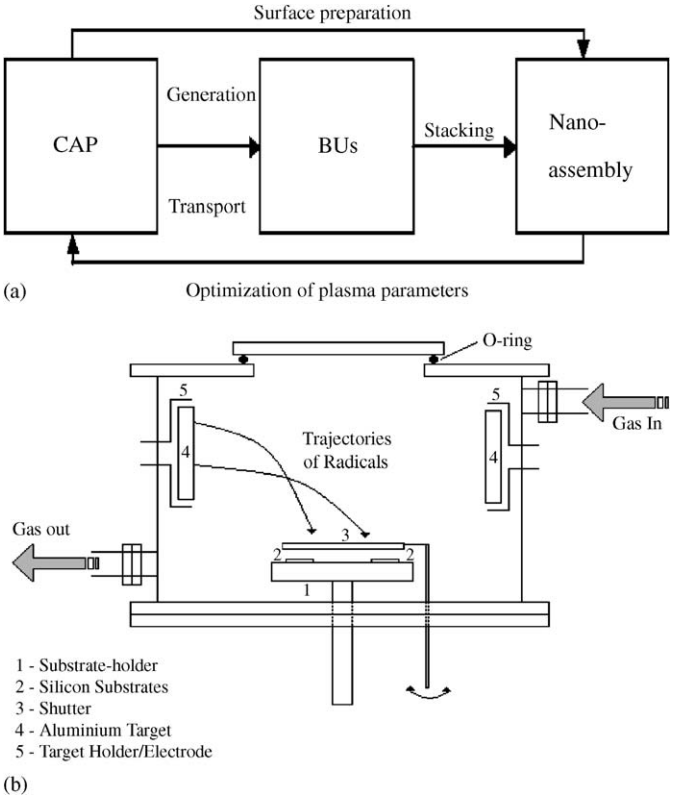

Fig. 1. Flow chart of the "cause and effect" approach (a) and schematic of the IPANF (b). CAP = chemically active plasma.

3. Integrated plasma-aided nanofabrication facility

The functional nanoassemblies of our interest here have been synthesized in custom-designed Integrated Plasma-Aided Nanofabrication Facility, a schematic diagram of which is shown in Fig. 1(b). This device encompasses the means of generation of highly uniform high-density plasmas by driving the external spiral (the rf coil is not shown in Fig. 1(b); it is installed above the quartz top end plate) or internal oscillating unidirectional rf currents, operation of low-pressure discharges in mixtures of reactive gases, control of deposition processes by using the substrate stages with the temperature- and deposition area- control functions, multiple rf sputtering targets (two of them are shown in Fig. 1(b)), and advanced diagnostic instrumentation. The internal rf coil can be installed by replacing the top quartz window by the top assembly that houses the internal rf antenna. This facility is suitable for large-area plasma processing due to its large (50 cm) internal diameter. The rf current is driven in either antenna configuration by a 460 MHz rf generator via an in-house designed matching network. The exact ranges of rf input power and parameters of the rf circuit to sustain the discharges in the required reactive gas feedstock and working pressure are estimated by using the results of our numerical simulations of the discharges sustained in reactive gases. To enable the efficient deposition of various thin films in the temperature-controlled regime, the moveable (in the vertical and azimuthal directions) substrate stage with a built-in thermocouple and external temperature control unit, is installed as shown in Fig. 1(b). An automated shutter (with or without any perforated pattern) enables one to partially cover any part of the surface being processed and control (e.g. focus) the ion/neutral fluxes from the plasma. Three equidistantly positioned (along the circumference of the chamber) 13.56 MHz rf magnetron sputtering electrodes enable the sequential and controllable release of the target material (e.g. Al, Fe, Ni, Co, In, Si, Ti, etc.) into the reactive gas environment. This technique is particularly useful in the plasma-assisted synthesis of various semiconductor quantum confinement structures and biocompatible films, as shown below. The advanced plasma diagnostic instrumentation includes Langmuir and magnetic probes, ultra-high-resolution optical emission spectroscopy (OES), and quadruple mass spectrometry (QMS). Further details of the plasma source operation (mostly relevant to the prototype versions), stability,

plasma diagnostics and parameters can be found elsewhere [7]. The IPANF can be operated in four regimes: (i) CVD mode (no plasma, heated substrate stage); (ii) magnetron sputtering mode (in argon); (iii) PECVD mode (in reactive gases); and (iv) combined PECVD and magnetron sputtering mode. For the synthesis of the CNTs, modes (ii) and (iii) are used consecutively, whereas assembly of low-dimensional semiconductor structures requires plasma-assisted sputtering of one or more solid targets (mode (iv)).

4. Applications

The aim of this section is to demonstrate the numerous applications of the IPANF and the "cause and effect" nanofabrication approach. Specifically, we have used the low-to-intermediate pressure (0.07–26.6 Pa) discharges in the following main combinations of reactive gas mixtures and sputtering materials:

- $Ar + CH_4/C_2H_2 + H_2$ for fabrication of various carbon-based nanostructures;
- $Ar + SiH_4 + H_2 + N_2$ (optional Ta, Ti) for deposition of silicon quantum structures and dielectric barriers;
- $Ar + N_2$ (optional) + [Al, In, Si, C, SiC, Ti, Ta, V, Er, etc.] + SiH_4 (optional) for fabrication of various semiconductor quantum dots and nanowires;
- Ar + Ti (optional) + H_2O (liquid precursor) + hydroxyapatite (HA) for fabrication of biocompatible calcium–phosphate-based coatings.

We emphasize that depending on the specific process requirements other reactive gases and sputtering targets can be used in the IPANF.

4.1. Carbon nanostructures

Arrays of carbon nanotip structures (Fig. 2(a)) were synthesized in $Ar + H_2 + CH_4$ plasmas at 5.32–6.65 Pa in the IPANF operation mode (iii) on highly doped Si(1 0 0) substrates pre-coated in situ by a thin nickel catalyst interlayer in the rf magnetron sputtering deposition mode (ii). The (negative) substrate bias and surface temperature were 80–150 V and 500–550 °C, respectively. In this process, a number of plasma-generated working species have a specific function. Specifically, Ar^+ ions are used for physical sputtering of residue contaminants from the chamber surfaces and direct plasma heating of the catalyst layer. H and H^+ species contribute to reactive chemical etching of the nickel layer and dynamic termination of carbon bonds that restricts the lateral nanotip growth [7]. Furthermore, radical CH_3 and cation CH_3^+ species are believed to be the main building units that incorporate into the growing carbon nanotip pattern. This is consistent with the results of atomistic simulations of equilibrium chemical structure of carbon nanotips by using ab initio Density Functional Theory (DFT) computations (Fig. 2(b)), Monte Carlo (MC) simulation of microscopic fluxes of CH_3^+ cation species onto ordered CNT patterns [8,9] and OES of the abundant plasma species in the growth process [7]. More specifically, the DFT computations show that the stable nanotip atomistic configuration is achieved when a CH_3 unit sits on the CNT top as can be seen in Fig. 2(b). It was previously shown [8] that hydrogen termination of a lateral surface is essential for the existence of the single crystalline structure shown in Fig. 2(c). On the other hand, the MC simulation results suggest that by varying the substrate bias, one can selectively control the deposition of the CH_3^+ BUs along the lateral surface of the growing nanotips, either closer to the tip or the substrate [9]. In the first case, the tips are sharper and longer, while in the

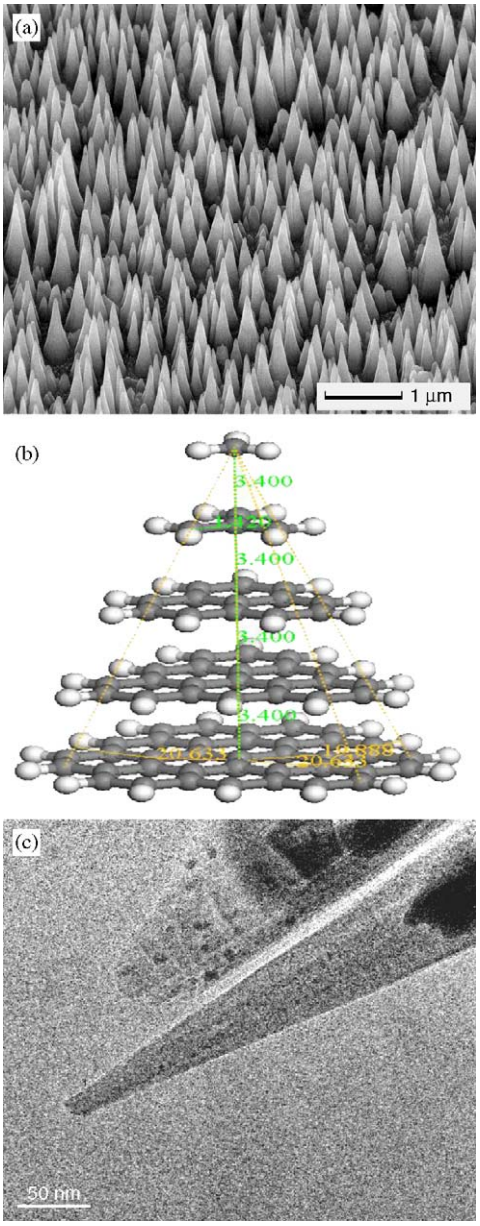

Fig. 2. Single crystalline carbon nanotip structures: (a) SEM nanopattern imaging; (b) equilibrium atomistic structure constructed by using ab initio Density Functional Theory; (c) high-resolution Transmission Electron Microscopy showing the single crystalline structure of a nanotip.

second case they are shorter and wider. This is consistent with our experimental observations suggesting that high-aspect ratio nanotip (“nanoneedle”) structures can be grown at moderate (negative) DC biases below 100 V, whereas nanopyramidal structures grow at substrate biases exceeding 150–200 V, when precipitation of carbon material in the area uncovered by the nanotips becomes excessive [7]. The dependence of the OES on the substrate temperature (not shown here) suggest a remarkable abundance of CH_3 radicals in the plasma among other important species, being atomic and molecular hydrogen, carbon dimer C_2, and C_3. However, the growth kinetics of the single crystalline CNTs is not completely understood and is a subject of our ongoing work.

Further process optimization requires maximizing the delivery of the BUs directly to the nanostructure being grown thus promoting the enhanced growth of the nanostructured phase and inhibiting that of the amorphous phase in the areas uncovered by the nanotips. To this effect, it would be beneficial to maximize the yield, in the gas phase, of charged CH_3^+ BUs, which can be driven by the sheath electric field that converges towards the sharp tips of the CNTs. However, one should be cautious so as not to over-accelerate the CH_3^+ cation BUs by large DC biases. In this case, the chance of their landing in the internanotip space (and thus of undesired buildups of a-C:H deposits) is higher.

4.2. Management of nanoparticle contamination in the growth of carbon nanostructures

In the synthesis of various carbon-based nanostructures, we faced the problem of nanoparticle (NP) contamination, which is quite common to a wide range of applications from semiconductor manufacture to materials processing. In our case, nano- and micrometer-sized particles grown in a reactive environment of hydrocarbon plasma discharges is the main source of contamination in the nanostructure growth process, which requires essentially subnanometer-sized building blocks, such as CH_3 and CH_3^+ of the previous subsection. Grown in the plasma bulk, such nanoparticles are transported towards the substrate and often are able to fall onto it, creating irregular piles on individual nanotip structures and entire nanopattern as can be seen in Fig. 3(a) [10]. The intensity of the nanoparticle fallout varies in a wide range depending on discharge conditions that determine the NP charge and dynamic force balance on the particles [11,12] . However, we have found efficient means of manipulating the plasma-grown nanoparticles by varying the neutral gas temperature gradient (TG) in the vicinity of the substrate [10]. This parameter is essentially plasma-independent and can be controlled by additional substrate heating. The variation of the TG results in notable changes in the size distribution of nanoparticles on the substrate, which was quantified by using the nanoparticle radius distribution function (NPRDF). The correlation between TG and NPRDF

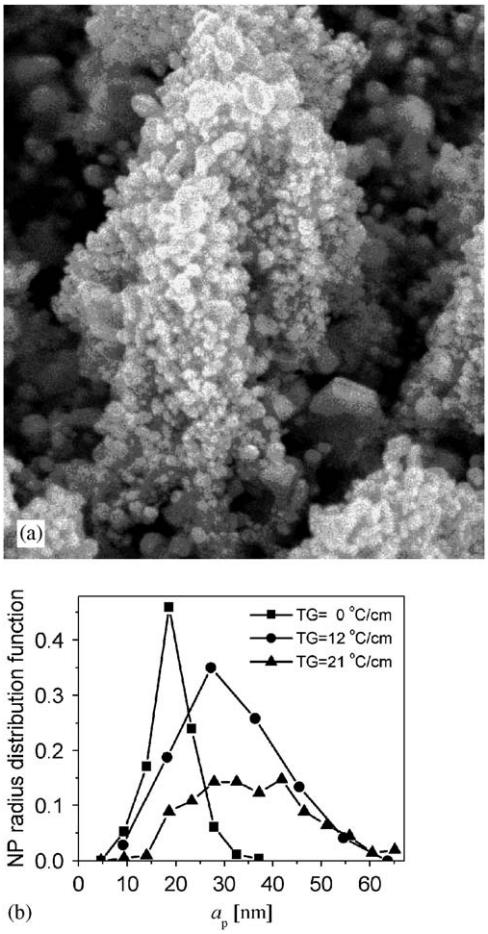

Fig. 3. Management of the plasma-grown nanoparticles in the synthesis of carbon-based nanostructures: (a) typical nanoparticle contamination over the carbon nanostructures; and (b) variation of the NRDF with the additional temperature gradient (TG) over the deposition substrate created by external substrate heating.

observed in our experiments is presented in Fig. 3(b). One can see that higher temperature gradients shift the NPRDF maximum towards larger radii and also broaden the distribution. Depending on the discharge parameters, the NPRDF peak position can change. However, the results remain very sensitive to the magnitude of the temperature gradient. A straightforward conclusion from this result is that for the TG exceeding certain threshold value, the deposited films can be completely free of nanoparticle contamination, similar to the structures shown in Fig. 2(a).

4.3. Low-dimensional semiconductor structures

We now discuss the use of our approach for the assembly of SiC QDs on Si(1 0 0) with AlN buffer interlayers synthesized in the IPANF. The AlN buffer layer (typically 10–20 nm thick) was pre-deposited on silicon substrates in situ by reactive rf magnetron sputtering of Al target in reactive nitrogen plasmas. Nanofabrication of SiC quantum dots structures (Fig. 4(a)) was performed by rf magnetron sputtering of SiC target in 3.46 Pa $Ar+H_2$

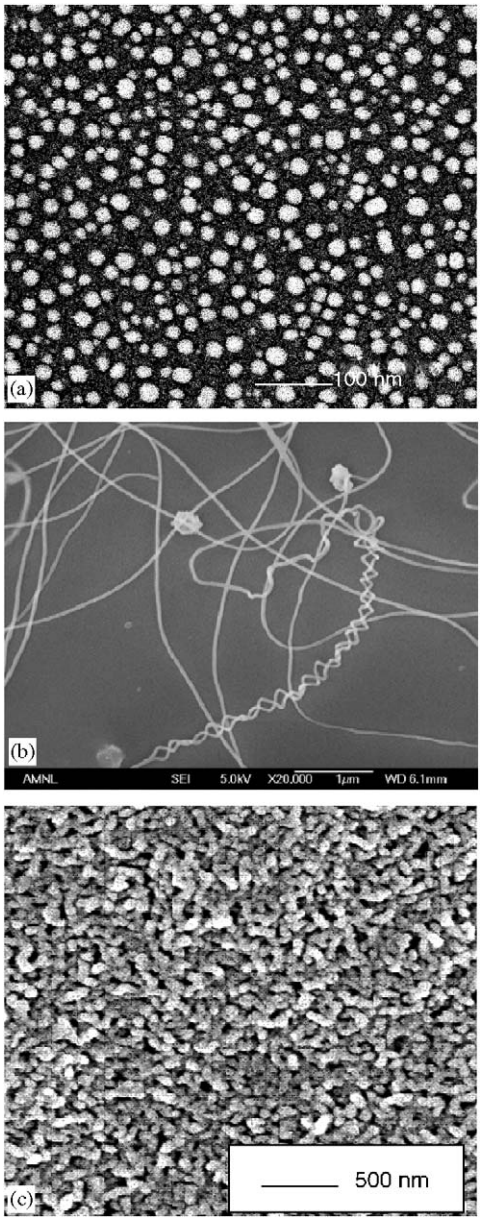

Fig. 4. Scanning Electron Microscopy of SiC quantum dot arrays (a), SiC nanowires (b), and nanocrystalline hydroxyapatite bioceramic (c) synthesized in the IPANF.

reactive plasmas (IPANF mode (iv)). Assuming the sputtering and ionization efficiency high, it is reasonable to assume that neutral or ionized silicon and carbon atoms are the most likely BUs in this case. The latter mostly incorporate into the quantum dots via surface migration following their deposition (adions are also neutralized on the surface) onto open surface areas. The results of simulation of growth of SiC QDs on AlN [13] suggest that the average QD size is ~13.5 nm and the surface coverage is ~0.19 for a typical deposition duration (~30 min), which is consistent with the experimental results. In the simulation, it was assumed that the SiC QD pattern grows from Si and C adatoms landed on and diffused over AlN surface and Si^+ and C^+ ions driven through the plasma sheath directly to the NA [13]. Even though these simulation results support our assumption on the main building blocks of the quantum dot arrays of our interest here, the simulation yields lower values of the average QD size (~13.5 nm) than in the experiments (~24.6 nm). A possible reason for this discrepancy is the limitations of the simulation model and arbitrary assignment of the plasma ionization degree, and hence, the proportions of the species incorporating in the growing NA via two different nanoassembly routes (directly from the gas phase and via the intermediate process of surface migration).

Alternatively, pre-depositing a nickel nanolayer (rf magnetron sputtering of a pure Ni target in the IPANF mode (ii)) and operating at slightly higher pressures (below 13.3 Pa) in the IPANF mode (iv), and adjusting the process parameters, one can fabricate ultra-high aspect ratio (~100–1000) SiC nanowires shown in Fig. 4(b). It is not clear at the moment which species is the dominant BUs for the SiC nanowire growth. Concerning silicon nanowires (that have also been synthesized in the IPANF mode (iii) by using $SiH_4 + H_2$ plasmas), it was recently argued that hydrosilicon clusters are the main BUs of silicon nanowires [14]. Indeed, when a nanocluster approaches from the short end of a similarly charged nanowire (both nanocluster and nanowire are expected to be charged negatively due to charging by highly mobile plasma electrons), the nanowire polarization is weak and the cluster is repelled. However, when the cluster approaches from the long end, the negative charge is pushed far away by the approaching cluster thus creating uncompensated positive charge near the growth end of the nanowire that effectively attracts the nanocluster. Our ongoing efforts are to develop a suitable numerical model of the nanowire–nanocluster interaction and a suitable nanocluster diagnostic tool to establish a correlation between the abundance of Si_xH_y nanoclusters in the gas phase and the growth dynamics of Si nanowires.

4.4. Biocompatible hydroxyapatite bioceramics

The deposition of biocompatible calcium phosphate-based films requires the concurrent/phase-in rf magnetron sputtering of hydroxyapatite and titanium targets in the low-to-intermediate pressure discharges in Ar (gas) + H_2O (liquid) feedstock (advanced IPANF operation mode (ii)) in which hydroxyl radicals (according to our approach they can thus be called ''functional units'') play a critical role in the enhancement of hydroxylation (hence, biocompatibility) of the bioceramic films. The bioinert Ti6Al4 V orthopedic alloy widely used for hip joint (and other) implants is used as a deposition substrate. The substrate bias and distance from the sputtering targets, the partial pressures of the gas mixture, and rf power supplied to the sputtering electrode can be independently adjusted to achieve the required film parameters, such as the [Ca]/[P] ratio of 1.67, which is the stoichiometric ratio of natural hydroxyapatite [15]. In particular, by sputtering the

Ti target, one can achieve the acceptable industrial standards for the interface bonding strength. By varying the (negative) bias, one can control the elemental presence in the films. Combined with the in situ optical emission and mass spectrometry measurements, these results suggest that the presence of calcium in the film is controlled by CaO^+ cation BUs. On the other hand, the abundance of P in the hydroxyapatite coating depends on number densities of phosphorus-containing radicals in the gas phase. The films feature excellent biocompatibility and porous structure as can be seen in Fig. 4(c). The implant coatings synthesized in this way also sustain an efficient ingrowth of HA material from the simulated body fluid. Further details of the plasma-assisted synthesis and biocompatible properties of hydroxyapatite can be found elsewhere [15].

5. Conclusion

Our results on the plasma-aided fabrication of carbon nanotip microemitter structures, semiconductor quantum dots and nanowires, and nanocrystalline bioceramic coatings of orthopedic Ti-based alloy by using an in-house developed integrated plasma-aided nanofabrication facility and following the "cause and effect" approach is just the first step towards the development of highly controllable and predictable nanofabrication strategies based on specific building units of the desired nanofilms and nanoassemblies. Meanwhile, the quality of the targeted nanopatterns turns out to be very sensitive to contamination by plasma-grown nanoparticles. Therefore, selective manipulation of different nanostructure building blocks and removal of unwanted contaminant species and nanoparticles is a microscopic route for plasma-aided deterministic nanofabrication.

Acknowledgments

The authors sincerely thank S. Y. Huang, Z. Tsakadze, I. Levchenko, and M. Xu for fruitful collaborations. This work was partially supported by the Australian Research Council, Agency for Science, Technology and Research (Singapore), the University of Sydney, and the International Research Network for Deterministic Plasma-Aided Nanofabrication.

References

[1] Roco MC, Williams S, Alivisatos P, editors. Nanotechnology research directions: vision for nanotechnology research and development in the next decade. Amsterdam: Kluwer Academic; 1999. See also: http://www.nano.gov.
[2] Poole CP, Owens FJ. Introduction to nanotechnology. New York: Wiley; 2003.
[3] Pitkethly MJ. Nano Today 2003;6:36.
[4] Oehrlein GS. Plasma processing of electronic materials. Berlin: Springer; 2003.
[5] Vladimirov SV, Ostrikov K. Phys Rep 2003;393:175.
[6] Ostrikov K. Rev Mod Phys 2005;77:489.
[7] Tsakadze ZL, Ostrikov K, Xu S. Surf Coat Technol 2005;191/1:49.
[8] Chua HL, Xu S. Proceedings of second international conference on nanostructures and nanotechnology, 25–26 November 2004, Singapore, paper T18.
[9] Levchenko I, Ostrikov K, Keidar M, Xu S, J Appl Phys 2005;98:064304.
[10] Rutkevych PP, Ostrikov K, Xu S. Phys Plasmas 2005;12:062105.
[11] Ostrikov KN, Vladimirov SV, Yu MY, Morfill GE. Phys Rev 2000;E61:4315.
[12] Ostrikov KN, Vladimirov SV, Yu MY, Morfill GE. Phys Plasmas 2000;7:461.
[13] Levchenko I, Ostrikov K. Proceedings of the "complex systems" conference, a part of the SPIE microelectronics, MEMS, and nanotechnology symposium, 11–14 December 2005, Brisbane, Australia. SPIE proceedings paper 6039-24.
[14] Hwang NM, Kim DY. Int Mater Rev 2004;49:171.
[15] Xu S, Long JD, Sim L, Diong CH, Ostrikov K. Plasma Proc Polym 2005;2:373.